Available online at www.sciencedirect.com
SCIENCE DIRECT®
Nuclear Instruments and Methods in Physics Research A 507 (2003) 622–635
NUCLEAR INSTRUMENTS & METHODS IN PHYSICS RESEARCH Section A
www.elsevier.com/locate/nima

An X-ray scanner for wire chambers

T. Akesson[a], E. Arik[b], K. Assamagan[c], K. Baker[c], D. Benjamin[d], H. Bertelsen[e], V. Bytchkov[f], J. Callahan[g], M. Capeans-Garrido[h], A. Catinaccio[h], A. Cetin[b], P. Cwetanski[h], H. Danielsson[h], F. Dittus[h], B. Dolgoshein[i], N. Dressnandt[j], W.L. Ebenstein[d], P. Eerola[a], P. Farthouat[h], D. Froidevaux[h], Y. Grichkevitch[k], Z. Hajduk[l], J.R. Hansen[e], P.K. Keener[j], G Kekelidze[f], S. Konovalov[m], T. Kowalski[n], V.A. Kramarenko[k], K. Kruger[h], B. Lundberg[a], F. Luehring[g], A. Manara[g], K. McFarlane[c], V.A. Mitsou[h,1], S. Morozov[i], S. Muraviev[m], A. Nadtochy[o], F.M. Newcomer[j], J. Olszowska[l], H. Ogren[g], S.H. Oh[d,*], V. Peshekhonov[f], M. Price[h], C. Rembser[h], A. Romaniouk[h,i], D.R. Rust[g], V. Schegelsky[o], M. Sapinski[l], A. Shmeleva[m], S. Smirnov[i], L.N. Smirnova[k], V. Sosnovtsev[i], S. Soutchkov[i], E. Spiridenkov[o], V. Tikhomirov[m], R. VanBerg[j], V. Vassilakopoulos[c], C. Wang[d], H.H. Williams[j]

[a] *Fysiska Institutionen, Lunds Universitet, Lund, Sweden*
[b] *Department of Physics, Bogazici University, Istanbul, Turkey*
[c] *Department of Physics, Hampton University, Hampton, VA, USA*
[d] *Department of Physics, Duke University, Durham, NC, USA*
[e] *Niels Bohr Institute, University of Copenhagen, Copenhagen, Denmark*
[f] *Joint Institute of Nuclear Research, Dubna, Russia*
[g] *Department of Physics, Indiana University, Bloomington, IN, USA*
[h] *European Laboratory for Particle Physics (CERN), Geneva, Switzerland*
[i] *Moscow Engineering and Physics Institute, Moscow, Russia*
[j] *Department of Physics and Astronomy, University of Pennsylvania, Philadelphia, PA, USA*
[k] *Moscow State University, Institute of Nuclear Physics, Moscow, Russia*
[l] *Henryk Niewodniczanski institute of Nuclear Physics, Cracow, Poland*
[m] *P.N. Lebedev Institute of Physics, Moscow, Russia*
[n] *Faculty of Physics and nuclear Techniques of the Academy of mining and Metallurgy, Cracow, Poland*
[o] *Petersburg Nuclear Physics Institute, Gatchina, St. Petersburg, Russia*

Received 27 December 2002; received in revised form 13 March 2003; accepted 27 March 2003

*Corresponding author. Tel.: +1-919-660-2579; fax: +1-919-660-2525.
E-mail address: seog@phy.duke.edu (S.H. Oh).
[1] Also at Physics Department, University of Athens, Athens, Greece.

doi:10.1016/S0168-9002(03)01389-5

Abstract

The techniques to measure the position of sense wires and field wires, the gas gain and the gas flow rate inside wire chambers using a collimated and filtered X-ray beam are reported. Specific examples are given using barrel modules of the Transition Radiation Tracker of the ATLAS experiment.

PACS: 29.40.Gx

Keywords: ATLAS; TRT; X-ray scanner; Wire position; Gain map; Gas flow

1. Introduction

Wire chambers have been one of the most important detector technologies since their invention about 30 years ago [1]. Over the years, many different wire chambers have been constructed and virtually every high-energy physics experiment has one or more types of these chambers. Experiments at the Large Hadron Collider (LHC) at CERN are no exception. In both ATLAS [2] and CMS detectors [3], there will be a large number of muon chambers and in ATLAS, one of the main inner trackers is a wire chamber, specifically, a straw tube chamber called Transition Radiation Tracker (TRT). It is likely that wire chambers will continue to play an important role even after the LHC period.

As chambers get more complicated and are expected to operate in higher radiation environments, new materials (low radiation length, radiation hard and less outgassing) are used in the chambers. In order to achieve the best resolution in extremely high rate environment with limited space, new electronics have been designed with lower power dissipation.

Another limiting factor for the resolution is accurate placement of the wires, both the field and sense wires and the chamber itself. Very elaborate schemes to monitor the position of chambers in real time are common today. For the best possible resolution, the wire positions are mapped and used in the reconstruction program. With a large number of sense wires, any mapping has to be done fast and efficiently.

Sometimes the wire chambers are used for purposes other than tracking. They are used for calorimeters, particle identification using $\mathrm{d}E/\mathrm{d}x$ or transition radiation. For these types of applications, uniform gain along the sense wire is an important factor. Before chambers are put in operation, gain variation within a wire and from wire to wire should be measured for a calibration.

For very high rate operation and aging, proper gas flow rate throughout a chamber is important. The chemicals produced near the sense wire may not get flushed out fast enough and result in different operating and aging characteristics. Careful design of the gas inlet and outlet locations can solve the problem. Although modeling the gas flow rate for a chamber would be possible, one should measure the flow rate throughout the chamber.

We have faced all these problems in developing the barrel TRT for ATLAS because the detector functions as a tracking device as well as a particle identification device using transition radiation. In this paper, we report on the techniques developed to solve the problems. We report on the techniques for measuring the wire position, gain and gas flow rate using a collimated and filtered X-ray beam. Although originally developed to check the quality of the TRT modules, they can be easily adapted for other types of wire chambers.

2. X-ray scanner

The X-ray machine used in the scanner is made by Pickard.[2] The maximum electron current is 10 mA with a maximum potential of 60 kV. The target is made of tungsten and has a beryllium

[2] The company Pickard is no longer in business.

window with a diameter of 5 cm. It produces a point-like X-ray source. The beam is collimated using a 100 μm wide, 2 cm long slit which is made of 0.63 cm thick brass. The collimator is attached to one end of a 35 cm long brass tube (0.63 cm thick and 5 cm outer diameter) and the other end is attached to the window, thus producing a beam of angular spread of 0.3 mrad. With the collimator assembly attached to the window, the radiation level around the X-ray source is quite low and no additional shielding is necessary.

The photon energy spectrum from an X-ray tube is well known. It is basically a $1/E$ distribution due to bremsstrahlung with peaks due to the discrete atomic energy levels (known as K, L,... peaks). In our application the collimated X-ray beam is filtered through a 50 μm thick copper sheet. The reasons are two fold. One is to stop any low energy electrons associated with the beam and the other is to narrow the X-ray energy spread using the K edge absorption. The X-ray spectrum entering a straw tube gas volume in the test chamber can be calculated using the transmission coefficients of material[3] between the X-ray window and the detector.

Fig. 1a shows the calculated energy spectrum after the X-ray beam passes through the material including the copper filter. For this distribution, photons with $1/E$ distribution are generated and plotted as a function of energy with weights calculated using the photon transmission coefficients. The weight is the product of transmission coefficients of various materials in the beam's path. The types of material used in the calculation include 35 cm of air, 50 μm of copper, 500 μm of carbon (material for the shell which houses the test module), and 60 μm of Kapton (straw tube material). The sharp drop near 9 keV is caused by the K edge absorption of the copper filter.

The X-ray tube with the collimator is placed on a support as shown in Fig. 2. The support is designed to move vertically (y-axis) to accommodate the different size chambers by adjusting the screws on four threaded rods. Below the X-ray

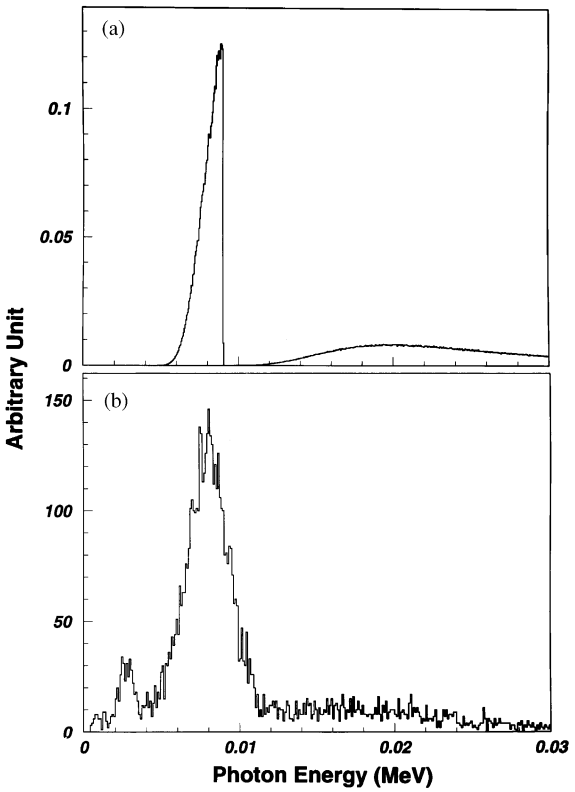

Fig. 1. (a) The calculated photon energy spectrum entering the ionization gas volume of a straw tube using the product of the photon transmission coefficients of various materials in the path of the X-ray beam. (b) The simulated detector response (with 4 mm diameter straw tubes) to the photon spectrum shown in (a) using the EGS program. The ionization gas is a mixture of argon and ethane (50%/50%).

machine, a chamber stand which can move in two directions (x- and z-axis) is made of two sliders attached to stepping motors.[4] The travel distance along the z-axis (along the straw tubes) is 160 cm and 15 cm along the x-axis (perpendicular to straw tubes). The dimensions are similar to the size of the ATLAS TRT barrel modules because the scanner was originally developed to scan the modules as a part of the production quality control. The accuracy and the repeatability of positioning the chamber stand are about 1 m along the x-axis and about 5 μm along the z-axis.

[3] There are several well-developed web sites for the general X-ray data, for example, http://X-ray.uu.se/, http://www.csrri.iit.edu/, http://www-cxro.lbl.gov and references therein.

[4] The sliders with stepping motors and the stepping motor controller are made by AeroTech, Pittsburgh, PA, USA.

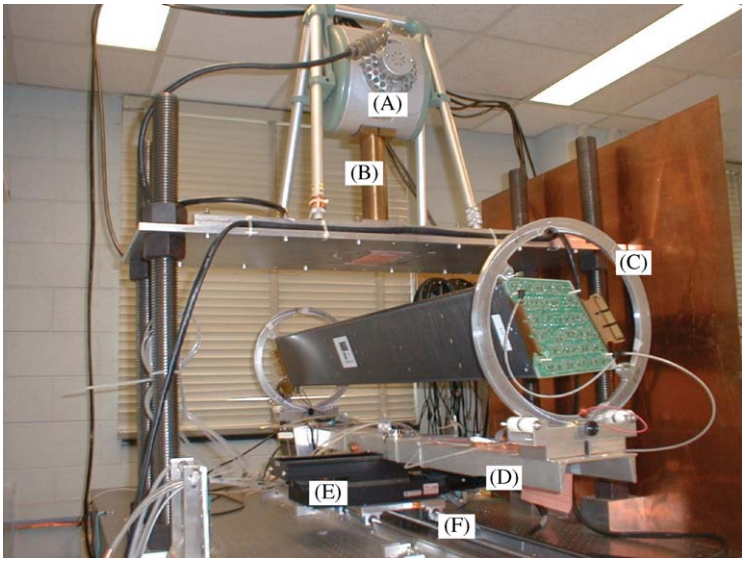

Fig. 2. A picture of the X-ray scanner. The X-ray tube is housed inside a casing (labeled A). The X-ray beam exit from a window at the top of the long brass tube (B), and the collimator is at the bottom of the tube. A module is attached to two circular rings (C) which are sitting on a long aluminum base plate (D). The plate is on the top of two sliders (E and F) attached to stepping motors controlled by the DAQ PC. One slider (E) moves the chamber along the x direction, and the other slider (F) moves the chamber along the z direction.

Although the entire assembly is on an optical table, the y-axis accuracy of the assembly is not critical since our measurements are not sensitive to the y position. The program to control the stepping motors is incorporated into the DAQ system for the chamber readout.

3. Test chamber and readout system

The chambers used to test the scanner are constructed with 4 mm diameter straw tubes and 30 μm gold-plated tungsten wires. There have been several reports on the construction and performance of this type of chamber and the detailed construction and design of the chambers can be found in the Ref. [4]. The two test chambers used here are the prototype modules for the barrel TRT detector for the ATLAS experiment. The dimensions of the larger (smaller) module are about $15 \times 15 \times 150\,\mathrm{cm}^3$ ($10 \times 10 \times 130\,\mathrm{cm}^3$) and there are 520 (329) straw tubes inside. The TRT detector serves as a tracking chamber and an electron identifier through TR. For the TR function, the space between straws is filled with polyethylene

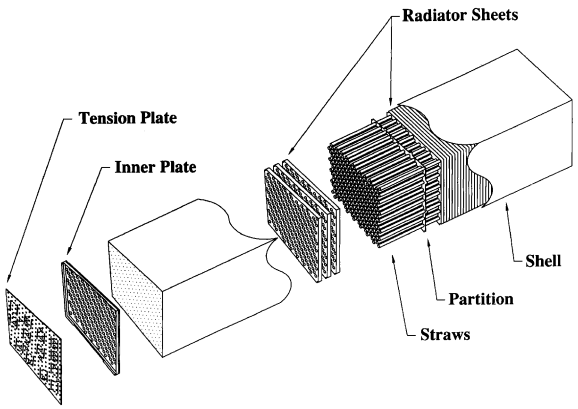

Fig. 3. An exploded view of the test chamber (a module). It is a barrel TRT module for the ATLAS experiment. The straw tubes end at the inner plate where they are glued to traces (not shown) using conductive glue. The traces are to provide HV to straws. Wires are fixed at the tension plates with 60 g of tension. See Fig. 15 for a detailed end assembly. The partitions (glued to the shell after being aligned with respect each other) are to align straws, and are located every 25 cm. The shell provides mechanical strength. The radiator sheets are to produce transition radiation photons for particle identification.

fibers of 20 μm diameter and density of $0.08\,\mathrm{g/cm}^3$. An exploded view is shown in Fig. 3. The module is supported off the $x - z$ slider by circular rings at

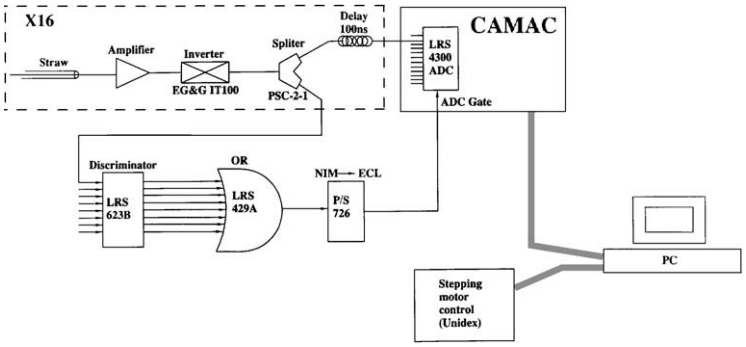

Fig. 4. The diagram for the electronics and DAQ system used in the experiment. See the text for a detailed description.

the ends, which are rotated to position the module with respect to the beam.

The diagram of electronics and readout system for the scanner are shown in Fig. 4. The signal from a sense wire is amplified and split two ways. The pre-amplifiers are the same ones used in the VTX chamber of CDF for Run I [5]. One part goes through a 100 ns delay line and is fed into a fast ADC (Lecroy FERA 4300). The other part is discriminated and ORed to generate a gate (150 ns width) for the ADC. Because of a lack of electronics, only 16 channels are read out at a given time. The readout system is based on CAMAC interfaced to a PC with a 400 MHz Pentium II processor. Since there is no hardware trigger to initiate the data taking, the Look At Me (LAM) of the ADC is continuously tested for the presence of data. While the event rate can easily reach 10 kHz (with 2 mA current and 35 kV setting, the default settings), the maximum data taking rate is limited by the DAQ speed and is about 3 kHz. By improving the DAQ readout system, the data taking speed could be easily increased by several times, which could be important if a large number of wires has to be scanned within a limited time.

The default mixture used for the chamber ionization gas is 50% argon and 50% ethane. With the amplifier and ADC, the high voltage (HV) is adjusted such that the peak of Fe^{55} source is at about 500 ADC counts, giving a corresponding HV of 1650 V.

Fig. 5a shows an energy spectrum taken with a Fe^{55} source, and Fig. 5b shows the same but with the X-ray source. Using the 5.9 keV Fe^{55} peak, the ADC channel numbers are converted to energies. As shown in the figure, the most probable photon

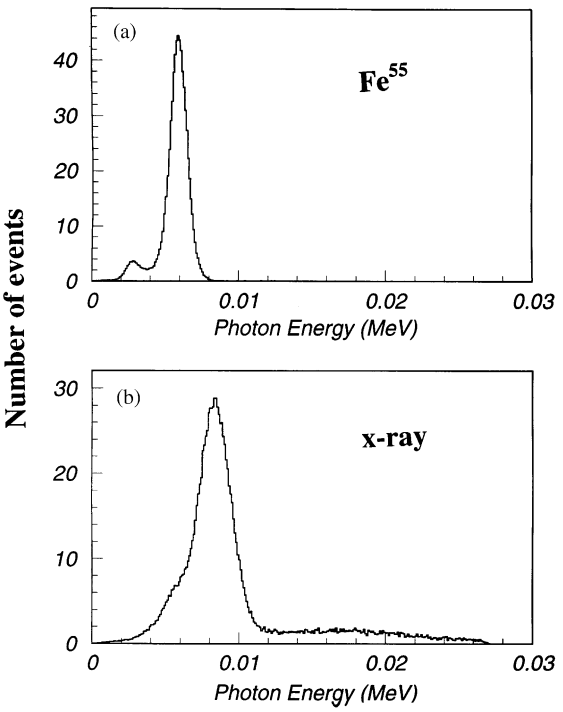

Fig. 5. (a) Energy spectrum with a Fe^{55} source. (b) Same as (a) but the source is the X-ray beam. The horizontal axis is a converted energy scale from the ADC channel number using the 5.9 keV Fe^{55} peak as a calibration point. The vertical axis is divided by 100. The gas is a 50%/50% argon–ethane mixture with the HV at 1650 V. The end point in the X-ray spectrum is due to the maximum ADC channel count.

energy produced from the X-ray beam is about 8 keV as expected. Although the X-ray spectrum shares the general features shown in Fig. 1a, the second broad peak in the data is somewhat smaller. This is because the interaction cross-section with ionization gas drops very rapidly as the X-ray energy increases. The dominating cross-section for the X-ray photons is the photoelectric effect at these energies.

The effect of the interaction cross-section can be simulated using the EGS simulation program [6]. In the simulation program, the photons are produced according to the spectrum in Fig. 1a and sent through a straw tube gas volume. If an electron is produced, its total energy loss inside the tube is obtained and plotted. The distribution in Fig. 1b shows the expected spectrum including the detector resolution of 13% calculated from the Fe^{55} spectrum (see Fig. 5a). The spectrum matches the data fairly well except at very low energies. It may be that the simulation does not handle the very low energy region properly.

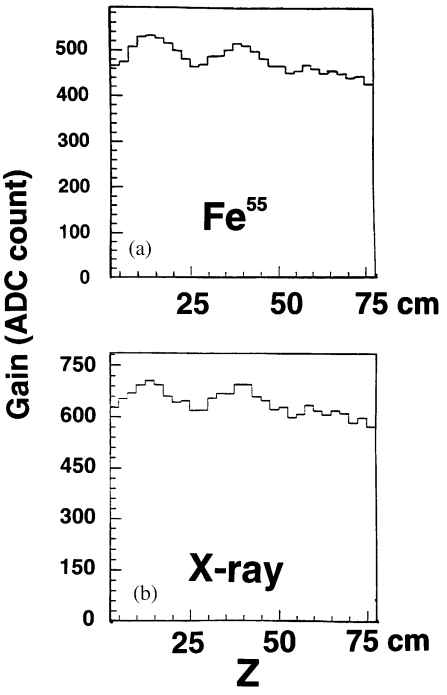

Fig. 6. (a) Gain measurement using Fe^{55} source. The vertical axis is the gain in ADC channel count and the horizontal axis is the distance along a straw tube. (b) Same as (a) but using the X-ray beam. Each point is the peak value obtained by fitting the peak in an ADC distribution (similar to Fig. 5) with a Gaussian function.

4. Gas gain variation measurement

The gas gain variation along a sense wire basically measures the non-uniformity of the electric field. The variation in the electric field is typically caused by improperly positioned sense wires and/or field wires (or straw tubes). Another reason could be the variation of sense wire thickness. The gain uniformity is important if a chamber is used in a calorimeter or as a transition radiation detector. Normally, the gain is measured using photons from a Fe^{55} radioactive source. However because the energy of the photons from Fe^{55} is low, they do not penetrate much material. The X-ray beam has an advantage of producing higher energy and intensity. In this paper, the gain refers to the relative gain not the absolute gain.

For the gain measurement, the slit is positioned (the long side) perpendicular to the sense wires. The chamber (mounted on the $x-z$ slider) is moved along the z-axis in 2 cm steps and the data is taken for 2 s. In order to verify that the gain measured using an X-ray source is not different from using an Fe^{55} source, the gain of a channel is measured using both sources along the length of a straw tube. Fig. 6a is from the Fe^{55} source and Fig. 6b is from the X-ray source. A channel with large gain variation was deliberately chosen for this study. In order to obtain the gas gain, the peak in each ADC distribution (similar to the one shown in Fig. 5) is fitted with a Gaussian function to obtain the mean of the peak. The mean is plotted as a function of z position. The mean after subtracting the pedestal is proportional to the gain. As shown in the figures, both sources produced comparable gain variation. The results are not unexpected since the energy of the filtered beam is well defined. We should point out that there is no attempt to measure the absolute gain in this experiment.

The relationship between the gas gain and the sense wire position in a straw tube has been

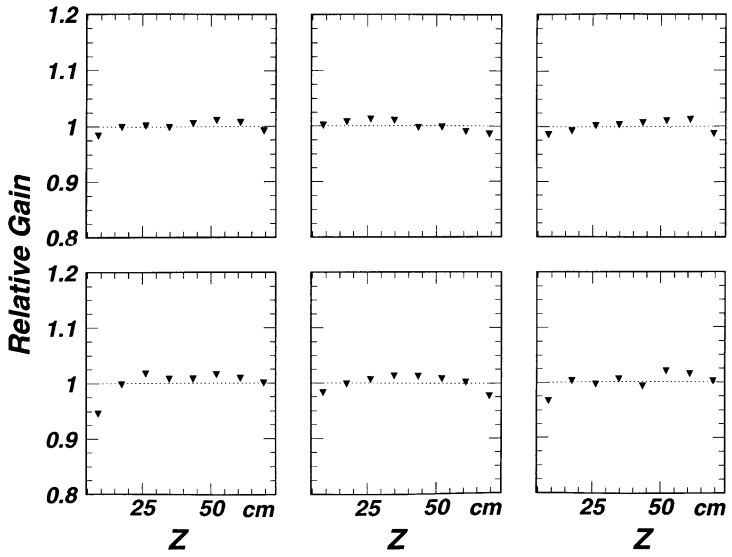

Fig. 7. The relative gas gain of six typical channels. The gains are normalized such that the overall average gain is 1.0. The statistical error is less than the size of the triangles. The uncertainty of data points is dominated by the repeatability which is $\sim$1.5%. This is mainly due to the environmental factors such as noise, temperature and pressure variation.

measured for different gas mixtures [7]. Typically, the gain increases by about 1% (2.5%) when the wire is shifted by about 100 (200) μm off center and the gain increase somewhat depends on the gas mixture. Although the gain measurement is not very sensitive to the wire position, it could provide quick and overall quality checks of a chamber. The gain variation for six typical channels from the test module is shown in Fig. 7. From the figure, we note that there are a few percent gain variations.

Because our beam is well collimated, another interesting measurement is the gain as a function of the drift distance from the sense wire. For this measurement the slit is rotated by 90° with respect to the previous measurement as illustrated in Fig. 8a. In Fig. 8b, the gain variation for every 100 μm step along the x-axis is plotted. The sense wire is at the valley of the distribution. The gain clearly decreases as the average drift distance decreases. This may be due to the different number of secondary electrons as the primary electrons drift toward the sense wire. We note that the actual gain near the wire should be much lower than the minimum at the middle of the data because the plotted gain is the averaged gain over the different drift distances (Fig. 8a). For example, when the X-ray beam is pointing to the edge of a straw tube (or to a sense wire), then the average drift distance is the tube radius (or a half of the tube radius). The edge in this paper is defined when $r \sim R_0$. R_0 is the tube radius and r is the distance from the sense wire along the x-axis.

5. Wire position measurement

One of the factors determining the resolution of a wire chamber is the wire position accuracy. We have reported a technique of measuring the wire position inside a low mass chamber using the electrons from a Sr^{90} radioactive source [8]. Because of the limited electron energy, this application is somewhat limited.

Using an X-ray source to map the wire position is not new [9,10]. In these schemes, the X-ray beam is scattered off a crystal to produce a mono-energetic beam. As the beam moves across a wire, part of the X-ray beam is scattered by the wire and results in a change of the counting rate. The

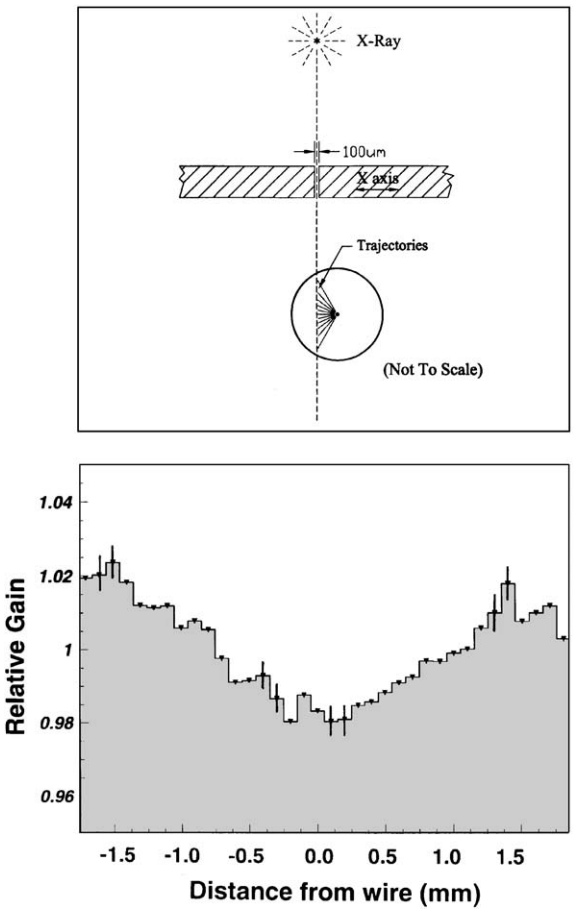

Fig. 8. (a) The slit position for Fig. 8b and the wire scanning. Also shown in the figure are the electron drift trajectories. (b) The gain variation as the X-ray beam moves along the x-axis (across a straw tube). The gains are normalized such that the overall average gain is 1.0. The size of error bars for all data points is similar and only some of them are shown.

counting rate can be done either in a passive way [9] or in an active way [10]. The passive way requires an external detector (typically a scintillator) and the active way reads out the rate directly from the straws. The counting rate is plotted against the beam position and the wire positions are calculated. It has been reported that the accuracy of this wire position measurement is better than 10 μm.

Our technique is based on a different principle. We have noticed that when the X-ray beam hits a wire, low energy electrons are emitted from the wire as shown in Fig. 9. The middle ADC distribution (Fig. 9b) is when the X-ray beam is passing between a sense wire and the edge of a straw tube ($r \sim R_0/2$). The distribution on the right (Fig. 9c) is when the beam hits a sense wire and there is an enhancement below the main peak. Simulation with EGS shows that the enhancement is caused by the knocked out electrons (photoelectric effect) from the wire surface. The distribution on the left (Fig. 9a) is when the beam is passing very near the edge of a straw tube ($r \sim R_0$). We also point out that it is not necessary to produce a mono-energetic beam for our measurement, thus the setup is simplified.

As a first step for the wire position measurement, the distributions like Fig. 10 are taken every 100 μm step across a tube. The slit is positioned along the z-axis. We define R as the ratio of the number of entries below the main peak (below ADC channel number 500) to the total number of entries in the distribution. This R is plotted as a function of the X-ray beam position and is shown in Fig. 10. There are three peaks. The one at the center corresponds to the wire position and the other two peaks are due to the straw walls. The peak values are found by fitting a Gaussian function with a flat background. In this technique, not only the wire position is measured but also the tube end wall positions. The wire is 30 μm diameter gold-plated tungsten wire and the straw tube is basically made of 50 μm thick Kapton [4]. It is important that the slit and the wires are aligned with an accuracy better than $\sim$100 m in order for the peaks in R distribution to show up well. This is done using an optical surveyor's instrument and the fiducial marks on the module and slit. It is worthwhile to point out that we only measure the projected wire position on the plane perpendicular to the X-ray beam direction. Because the beam direction is vertical, the sag due to gravity is not measured. For a three-dimensional mapping, the chamber has to be rotated (preferentially by 90°) and mapped one more time. The sag due to gravity can be easily calculated and added for the final wire position.

The accuracy of this technique is determined by measuring the position of a number of wires, translating the chamber by a known amount, and re-measuring the wire position. The shift is

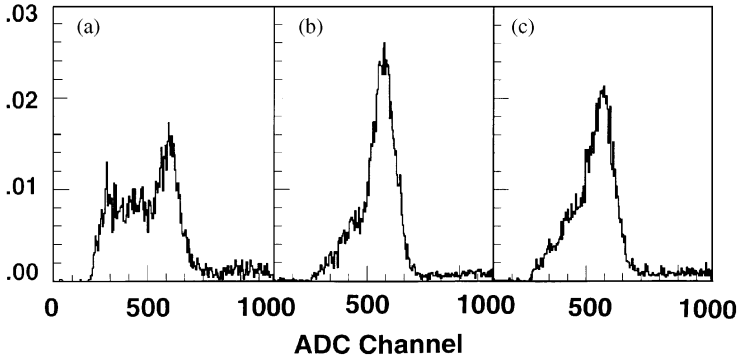

Fig. 9. (a) This distribution is obtained when the beam is pointing near the edge wall of a straw tube ($r \sim R_0$, R_0 is the tube radius and r is along the x-axis. (b) This is when the X-ray beam is between a sense wire and the edge of a straw tube ($r \sim R_0/2$). (c) This is when the beam hits a sense wire. The horizontal axis is the ADC channel number and the area of each distribution is normalized to 1.

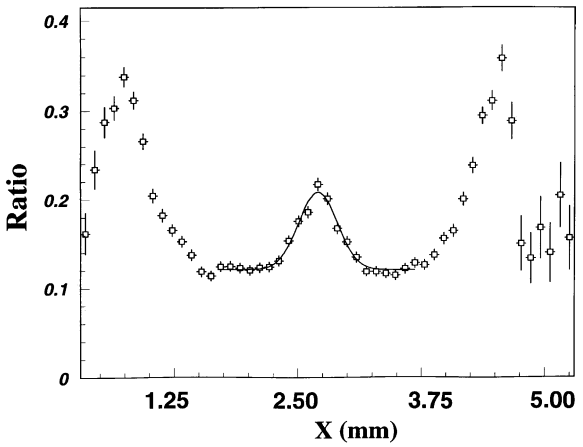

Fig. 10. A R plot. The points are calculated from the distributions shown in Fig. 9 by dividing the number of entries below the ADC count 500 by the total number of entries. Errors are statistical only.

measured using a digital dial gauge with resolution of 10 m. Fig. 11 shows the difference between the X-ray measurements and dial gauge measurement for three different shifts, 100, 200 and 300 μm. Fig. 11a shows the differences for eight wires separately and Fig. 11b shows all wires together. From the distribution, we conclude that the wire position can be measured to better than 20 μm ($25/2^{1/2}$, the error due to the dial gauge is ignored.).

The accuracy of the straw end wall position (and similarly for the straw inner diameter) determination is complicated because we do not know the exact location to which the leftmost and rightmost peaks in Fig. 10 correspond, since the projected

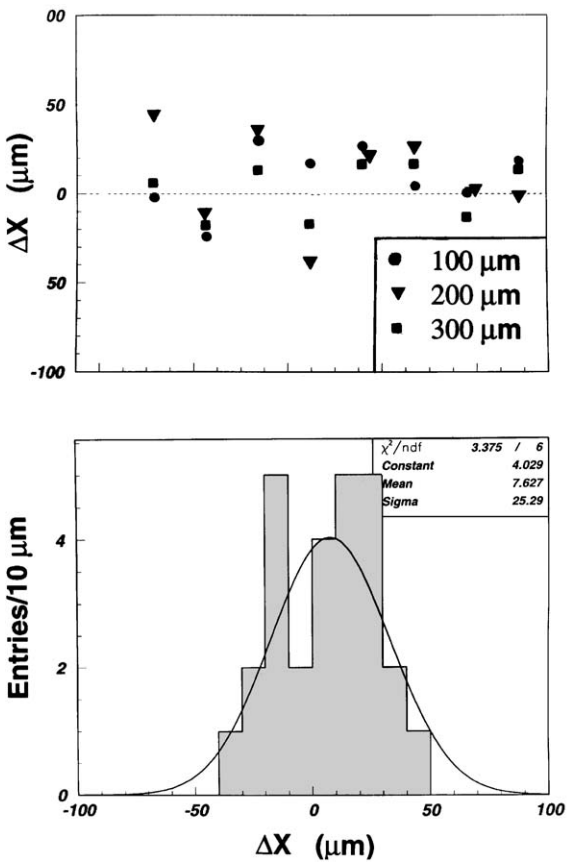

Fig. 11. (a) The difference in the wire position (Δx) between the X-ray measurement and dial gauge measurement after the chamber is translated by 100, 200 and 300 μm for eight different channels. The statistical error of each point is less than 10 μm. (b) This distribution is a projection of Fig. 11a to the vertical axis. From the distribution, we estimate that the accuracy of our wire position measurement is better than 20 μm.

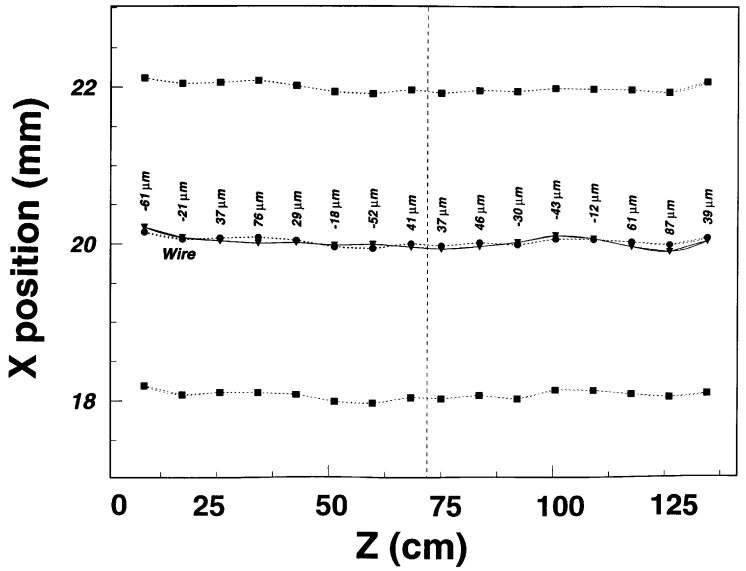

Fig. 12. The measured wire position (connected with a solid line), and the two straw wall edge positions (two dotted lines, one at the top and the other at the bottom) as a function of z position (along the straw tube length). Also plotted (dotted line in the middle) is the center of the two straw tube walls calculated by adding the two wall positions and dividing by two. The difference between the two curves (solid line and middle dotted line) is the wire offset with respect to the center of the straw tube. The magnitudes of the differences are also shown as text.

wall thickness varies continuously. However, using the average distance between the two peaks (3.85 ± 0.01 mm) and comparing it with the known straw tube diameter (4.00 ± 0.02 mm), we deduce that the peaks correspond to the locations slightly inside the straw inner wall by about 0.075 mm. Assuming the inner end wall positions can be calculated from the peak locations (by adding 0.075 mm to the peak positions), we estimate that the straw end wall positions can be measured with about 50 μm accuracy following the similar procedure for the wire accuracy estimation.

By adding the two straw end wall coordinates and dividing by two, and comparing this value to the corresponding wire coordinate, the deviation of the wire with respect to the straw center is calculated. Fig. 12 shows a distribution of the coordinates of a sense wire and the two straw end wall locations every 8 cm along the wire. Also plotted is the center of straws calculated as just described. The data points for the sense wire do not form a straight line because the slider moving along the z-axis is not exactly straight. The figure indicates that the straightness of the device is an order of 100 μm. Although it is desirable to construct a perfect device, the exact straightness is not necessary because the deviation (from a straight line) can be calculated and corrected from the fact that a (sense) wire fixed at two points is straight between the two points (see Fig. 14a).

We have studied the effect of different gas mixtures on R. Fig. 13a shows an R distribution taken with an argon/ethane (35%/65%) mixture and Fig. 13b shows the same with an argon/CO_2 (70%/30%) mixture. The HV is adjusted such that the gain is about the same for all mixtures. As shown in the figures, including Fig. 10, R distributions are insensitive to the type of gas mixtures.

This technique does not measure the absolute wire location (with respect to an external fiducial mark). In order to measure the absolute location, an external reference chamber with known wire position with respect to a fiducial mark is necessary. The external reference chamber could be another wire chamber, whose length could be

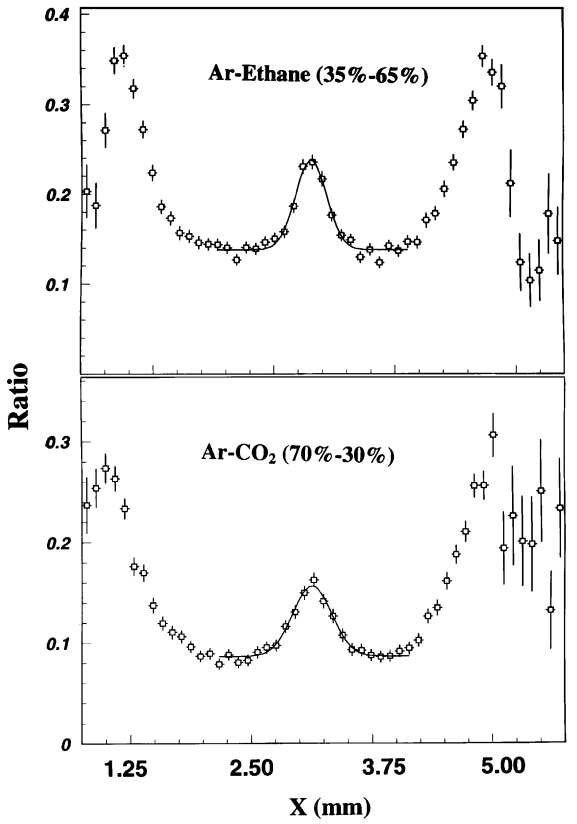

Fig. 13. A R distribution with a 35%/65% argon–ethane mixture (upper distribution) and 70%/30% argon–CO_2 mixture (lower distribution). Together with Fig. 10, there is not much dependence on the gas composition.

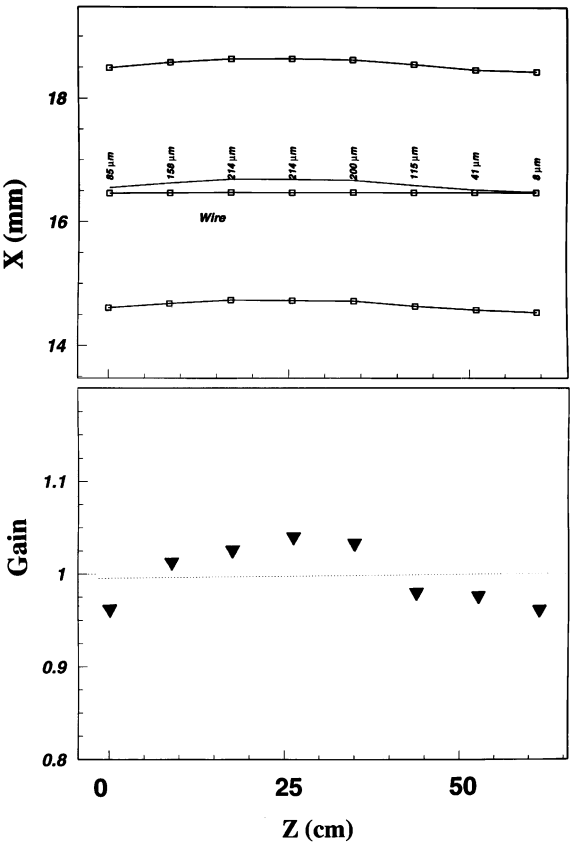

Fig. 14. (a) The wire and straw wall positions measured from a straw tube where the wire is off-centered. The data points are shifted such that the wire data points form a straight line. (b) The gain is plotted for the same straw tube. In both distributions the horizontal axis is distance along the straw tube.

slightly longer than the slit length. This chamber is fixed with respect to the beam near the chamber to be scanned and both chambers are scanned at the same time. The external fiducial mark on the reference chamber should be measured optically with respect to the wires in the reference chamber, thus the scanned wires can be referenced to the fiducial mark.

Fig. 14a shows an example in which the sense wire is not centered along the length of a section of a straw tube. It is off-center by about 200 μm in the middle. In this figure, the data points are shifted such that the sense wire is in a straight line. A detailed gain map along the straw tube is shown in Fig. 14b for a comparison and there is about 4% of gain variation where the offset is maximum.

This technique can also be applied for measuring the field wires inside an open type drift chamber. Low energy electrons produced when the X-ray beam hit a field wire would drift to a sense wire and be detected in a similar fashion.

One of the limiting factors of this technique is the penetration depth of the X-ray beam. The test chamber was designed for tracking as well as transition radiation detection. For the TR function, the space between straws is filled with radiator material and the wire position can be mapped only up to $\sim$10 cm depth. For other chambers without TR material, the scanning depth should increase. The depth of the scan can also be

increased by using a different filter. For example, a Ge filter rather than Cu will increase the main X-ray energy component by ~20%.

Another limitation arises when wires are stacked up along the direction of the X-ray beam. Because the attenuation length of 8–9 keV photons is about 4 μm in tungsten, a sense wire with any reasonable thickness completely blocks out photons. Thus, in order to measure the stacked up wires, they have to be offset at least by ~1 wire diameter. In most chambers this can be accomplished by slightly tilting the chamber with respect to the X-ray beam.

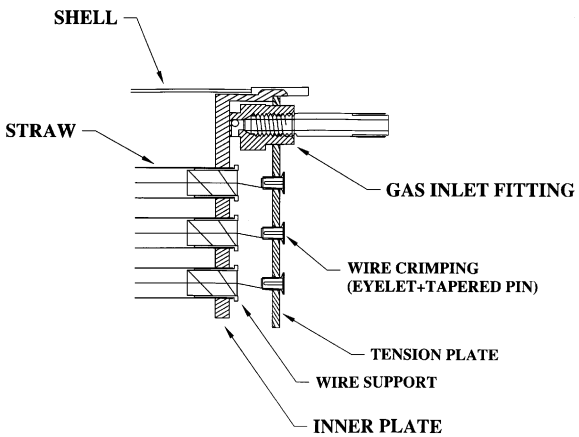

Fig. 15. A typical gas feeding system for a straw chamber. Because straws are isolated from each other the gas is fed in parallel from one end and taken out from the other end.

6. Gas flow rate measurement

The uniform gas flow through any chamber is an important consideration when gas inlets and outlets are designed. Some studies show that stagnated gas could accelerate the aging effect. The design is especially important for the chambers with straw tubes because straws are isolated from each other along their length. The typical gas feed system for chambers based on straw tubes is to supply gas to all tubes in parallel (Fig. 15). In this type of design, it is possible that there are straws with low gas flow, especially the ones at the corners. Although it may be possible to model the gas system and calculate the flow rate in each tube, it is still necessary to measure the actual gas flow rate in some tubes to verify the calculation.

The principle of measuring the flow rate is to detect the gain change as the gas composition changes. The gas gain is quite sensitive to the gas composition. For example, in Fig. 16, the relative gain is plotted as a function of the fraction of argon in an argon–ethane mixture. The points are normalized with respect to the gain obtained with 50% argon and 50% ethane. When the argon fraction changes by ~1%, the gain changes by ~6%.

After the chamber is flushed with a mixture (typically 50% argon and 50% ethane mixture), then the mixture is slightly changed (to 51% argon

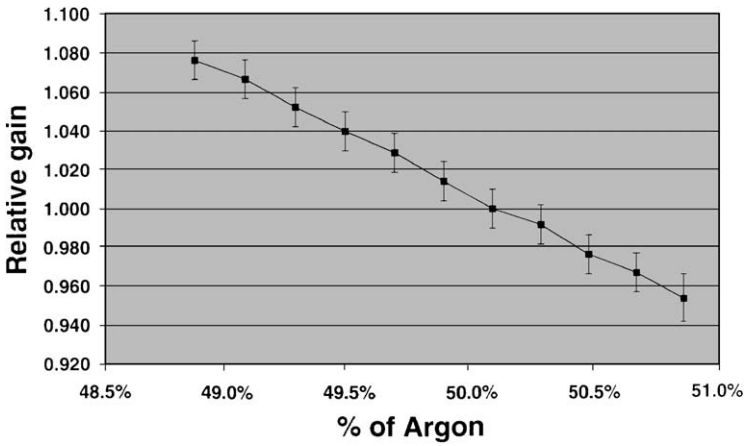

Fig. 16. The gas gain variation as a function of argon fraction in the argon–ethane mixture. The data points are normalized to the 50%/50% mixture.

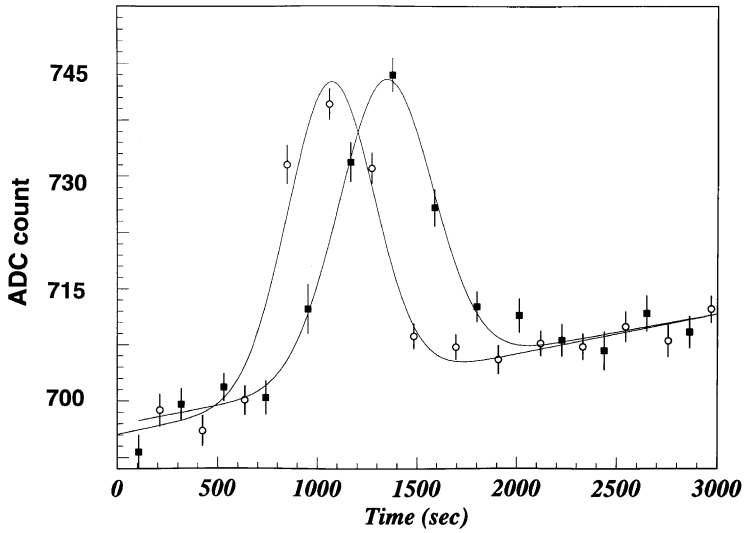

Fig. 17. The gain distribution in two locations separated by 20 cm as a function of time as the gas composition changes (from 50%/50% to 49%/51%) and returns to the original mixture (50%/50%). The slight slope in the baseline is due to our inability to return to the original gas mixture exactly.

and 49% ethane) for a period of time (typically for 5 min). After the period, the gas mixture is switched to the original mixture, thus producing a square wave of a different mixture. During the time, the gain of wires is measured at two locations separated by 20 cm along the tubes.

A typical signal amplitude distribution as a function of time is shown in Fig. 17. The horizontal axis is the real time in seconds. There are two distributions corresponding to the two locations. The jump in the gain signals the arrival of the different gas mixture. From the distributions, the peaks are found and the time difference between two peaks is calculated. The distance between two positions is divided by the time difference and the speed of gas flow is finally calculated.

Figs. 18a and b show lego plots of gas flow rate in each tube for two different flow rates. One is for 0.3 cm^3/min/straw and the other is for 0.5 cm^3/min/straw. The rate is calculated by simply dividing the total gas input rate to the module by the total number of straw tubes in the module. Using 0.12 cm^2 for the cross-section area of a straw tube, the flow rate 0.3 cm^3/min/straw corresponds to 2.5 cm/min for the gas speed. In the module used for the gas rate flow study (smaller of the two), there is one gas inlet and one outlet. The inlet locations are pointed out in the figures. The gas is fed to the module through a 0.3 cm diameter tube and the corresponding gas speed in the feeding tube is about 1400 cm/min for 0.3 cm^3/min/straw flow rate. As can be seen in the figure, the average gas flow rate from the measurement matches the expected flow rate and there is some variation in the flow rate among straws. It is interesting to note that the flow rate in the straws near the gas inlet is not much different from the straws far from the inlet even with one inlet.

This technique can also be used for open type drift chambers (with one large gas volume). Using a similar technique, one could map the mixing rate of ionization gas throughout a chamber and identify regions with low gas exchange.

7. Conclusions

In this paper, we have presented techniques for measuring wire position, gas gain and gas flow rate using a collimated and filtered X-ray beam. One advantage of using an X-ray machine is that it generates a controllable high intensity and high energy beam. The measurements can then be

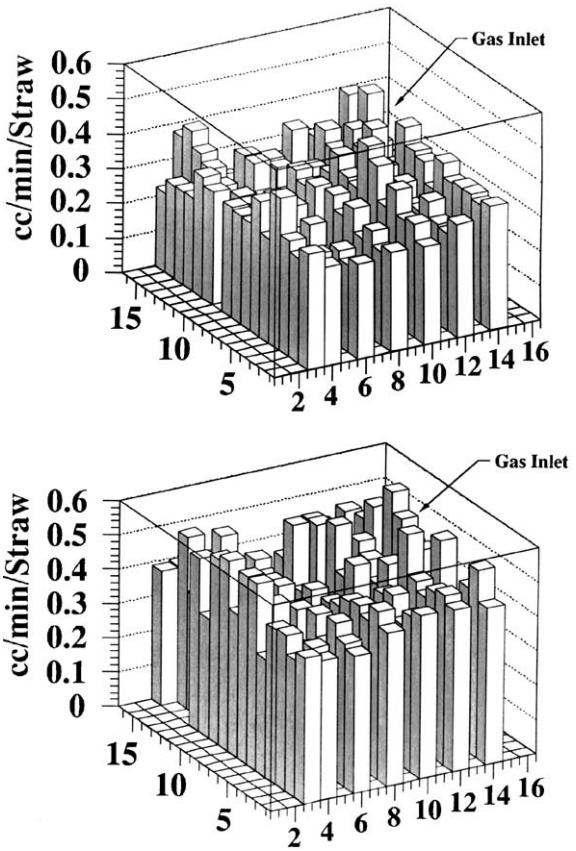

Fig. 18. A lego plot for the gas flow rate. The x- and y-axis correspond to the approximate straw tube positions in the module and the z-axis is the flow rate per minute. The physical size of one axis is about 10 cm. The top (bottom) data is taken when the average gas flow rate to the module is 0.3 (0.5) cm^3/min/straw. The location of gas inlets is indicated in the figures. The statistical errors for the data points are about 10–15%.

performed quickly with proper readout electronics, thus providing valuable information on the chamber quality in short time.

Among the techniques, first we have shown that a filtered X-ray beam can be used to measure the gas gain and the results are comparable to using a Fe^{55} source. The gain measurement provides important information on the uniformity of the electric field configuration. The gain measurement along the wire can be converted to a calibration table if chamber performance depends on the gain uniformity.

Second, we have demonstrated that the wires (sense and field wires) inside a chamber can be surveyed with accuracy better than 20 m. The technique of finding the wire location is to detect low energy electrons when the X-ray beam hits a wire. We have also shown that the straw walls can be accurately located. The location of wires can be input to a reconstruction program for better track momentum resolution.

Third, we presented a technique to measure the gas flow rate, which can be used for not only straw tube based chambers but also open type chambers. In the flow rate measurement, the gas composition to a chamber is changed slightly and the gain change due to the different gas composition is measured as a function of time. The flow rate measurement can locate regions where the gas exchange is low thus providing information for the proper gas inlet and outlet locations and/or the number of gas inlets and outlets.

References

[1] G. Charpak, R. Bouclier, T. Bressami, J. Favier, C. Zupancic, Nucl. Instr. and Meth. A 62 (1968) 235.
[2] ATLAS Technical Proposal, CERN/LHCC/94–43, CERN, 1994.
[3] CMS Technical Proposal, CERN/LHCC/94–38, CERN, 1994.
[4] ATLAS collaboration, ATLAS Inner Detector Technical Design Report, CERN/LHCC/97–17, ATLAS TDR 5, 1997.
[5] R. Yarema, IEEE Trans. Nucl. Sci. NS-33 (1986) 933.
[6] W.R. Nelson, H. Hirayama, D.W.O. Rogers, SLAC-265, 1985.
[7] P. Cwetanski, A. Romaniouk, V. Sosnovtsev, Studies of wire offset effect on gas gain in ATLAS TRT straw chamber, ATL-INDET-NO-2000-016 (ATLAS internal note for the inner tracking detector, http://cdsweb.cern.ch), 2000.
[8] S.H. Oh, C. Wang, M. Yin, Nucl. Instr. and Meth. A 325 (1993) 142.
[9] O. Fedin, S. Muraviev, A. Smirnov, 1994, ATLAS INDET-NO-057;
L. Vertogradov, ATLAS MUON-NO-041 (ATLAS internal note for muon detector, http://cdsweb.cern.ch), 1994.
[10] T. Akesson, et al., Nucl. Instr. and Meth. A 463 (2001) 129.